NACA

RESEARCH MEMORANDUM

FORCE AND PRESSURE CHARACTERISTICS FOR A SERIES OF
NOSE INLETS AT MACH NUMBERS FROM 1.59 TO 1.99

IV - CONICAL-SPIKE EXTERNAL-INTERNAL COMPRESSION

INLET UTILIZING PERFORATED COWL

By Robert T. Madden and Emil J. Kremzier

Lewis Flight Propulsion Laboratory Cleveland, Ohio

NATIONAL ADVISORY COMMITTEE FOR AERONAUTICS

March 28, 1951 Declassified July 17, 1958

NATIONAL ADVISORY COMMITTEE FOR AERONAUTICS

RESEARCH MEMORANDUM

FORCE AND PRESSURE CHARACTERISTICS FOR A SERIES OF NOSE INLETS

AT MACH NUMBERS FROM 1.59 TO 1.99

IV - CONICAL-SPIKE EXTERNAL-INTERNAL

COMPRESSION INLET UTILIZING PERFORATED COWL

By Robert T. Madden and Emil J. Kremzier

SUMMARY

As part of a general investigation of supersonic inlets in the NACA Lewis 8- by 6-foot supersonic wind tunnel, tests were conducted to determine the force and pressure-recovery characteristics of a model utilizing a single-shock spike-type inlet with a perforated cowl. External and internal pressure distributions, pressure recovery, and lift, drag, and pitching moment were measured for a range of mass-flow ratios at angles of attack from 0° to 10° for free-stream Mach numbers of 1.59, 1.79, and 1.99. The average Reynolds number based on the inlet diameter was approximately 2.4×10⁶.

The use of a perforated cowl resulted in the attainment of a high pressure recovery at zero angle of attack, but was accompanied by a relatively large increase in external drag as compared with nonperforated inlets of the same proportions. Throughout the range of stable operation, the total-pressure recovery decreased with increasing angle of attack, particularly at Mach numbers of 1.79 and 1.99.

Stable flow was observed at the design Mach number of 1.79 for the higher mass flows at zero angle of attack. The range of mass-flow ratios with stable operation decreased with increasing angle of attack and at 10°, shock oscillation was observed for all but the supercritical mass flow.

The calculated average subsonic-flow coefficient of the perforations for a free-stream Mach number of 1.79 and zero angle of attack was 0.53.

INTRODUCTION

The use of perforations in an inlet to obtain efficient supersonic diffusion has been investigated and is reported in references 1 to 3. The results of these investigations show that high pressure recoveries can be attained at zero angle of attack. Increases in drag, however, are also associated with these high pressure recoveries and must be taken into consideration in the evaluation of the performance of a perforated inlet. In order to compare the performance of a perforated inlet with that of other types of supersonic inlet, a single-shock conical-spike external-internal compression inlet utilizing a perforated cowl was investigated at the NACA Lewis laboratory in the 8- by 6-foot supersonic wind tunnel.

The inlet was attached to an afterbody, which formed the subsonic diffuser, and was investigated through a range of mass flows and angles of attack from 0° to 10° at Mach numbers of 1.59, 1.79, and 1.99. In addition to the determination of drag and pressure recovery, lift and pitching-moment characteristics were also obtained. The average Reynolds number was approximately 2.4×10⁶ based on the model inlet diameter.

SYMBOLS

The following symbols are used in this report:

- A perforated area
- C_D drag coefficient, D/q_0S_m
- C_{T.} lift coefficient, L/q_OS_m
- C_M pitching-moment coefficient about base of model, G/q_0S_ml
- c_p pressure coefficient, $p-p_0/q_0$
- D drag
- d diameter at area of maximum cross section, 8.125 inches
- G pitching moment about base of model
- L lift

- length of model, 59.149 inches
- M Mach number
- m mass flow
- P total pressure
- p static pressure
- q dynamic pressure, $\gamma pM^2/2$
- S area
- Sc inlet capture area defined by cowl lip, 0.1704 square foot
- S_m maximum cross-sectional area, 0.3601 square foot
- U velocity
- u velocity in boundary layer
- v_x axial perturbation velocity
- x,r,θ cylindrical coordinates
- y distance from model surface
- angle of attack
- γ ratio of specific heats
- δ boundary-layer thickness
- μ absolute coefficient of viscosity
- ρ mass density

Subscripts:

- l local condition in boundary layer
- T throat of inlet

- O free stream
- l cowl lip
- station at x = 7.688 inches
- 3 entrance to combustion chamber
- 5 minimum area at plug

APPARATUS AND PROCEDURE

Because the apparatus and procedure were, in general, similar to those of references 4 to 6, only the significant differences are discussed herein.

A photograph of the pressure model is shown in figure 1 and a schematic diagram of the complete ram-jet configuration is presented in figure 2(a) with the details of the inlet shown in figure 2(b). The coordinates for the entire model are given in table I.

The inlet was designed so that the oblique shock wave from the $40^{\rm O}$ cone would intersect the cowl lip at a free-stream Mach number of 1.8. As shown in figure 3, internal contraction was incorporated (S $_1/{\rm S}_T$ = 1.188) to reduce the average supersonic Mach number behind the oblique shock to approximately sonic velocity for the shock-swallowed condition at $\rm\,M_{\odot}$ of 1.79.

A method of calculating the perforation area necessary to allow the normal shock to swallow is given in reference 2. With a spike-type inlet, however, the existence of an appreciable boundary layer along the spike causes an effective reduction in throat area necessitating an increase in perforation area over that calculated by the method of reference 2. Because the displacement thickness of the boundary layer was unknown, the perforation area required for normal shock entrance was determined experimentally from the pressure model. A curve of the ratio of the summation of perforated area to throat area as a function of the ratio of diffuser area to throat area as determined from the pressure model is presented in figure 4. The force model was investigated using the perforation distribution as determined from the pressure model.

The locations of the static orifices on the pressure model are given in table II. Pressure orifices (taps) were not incorporated over the cowl because of the possibility of aerodynamic

NACA RM E51B05 5

interference between the instrumentation and the perforations. The strain-gage balance and angle of attitude indicator were similar to those described in reference 4.

The designation of the various axial stations along the model length used as subscripts in the notation of this report is shown in figure 5.

The tests with the force model covered a range of mass-flow ratios and angles of attack from 0° to 10° at Mach numbers of 1.59, 1.79, and 1.99. The pressure model was investigated at only a Mach number of 1.79 for the same angle-of-attack range.

RESULTS AND DISCUSSION

Characteristics at Zero Angle of Attack

External flow characteristics. - Changes in the shock pattern with varying amounts of mass spillage are shown in the typical schlieren photographs in figure 6. With the normal shock just inside the cowl lip (fig. 6(b)); m_3/m_0 , 0.871), the mass spillage produced shock waves that were nearly normal to the surface; whereas with the shock downstream of the perforations (fig. 6(c); maximum m_3/m_0 , 0.956), the smaller spillage produced only oblique shock waves. At lower mass-flow ratios, the shock pattern associated with additional mass spillage around the outside of the cowl lip is shown in figure 6(a).

The variation of total-drag coefficient with mass-flow ratio as measured with the force model is presented in figure 7. The total drag as obtained from this investigation includes the pressure and friction forces on the external shell and on the internal surface of the shell from the cowl lip to the downstream end of the perforated region and includes the pressure force along the limiting streamline of the mass flow passing through the unit (S_0 of fig. 5).

The adverse effect on the total drag of increasing mass-flow spillage through the perforations is indicated by the rapid increase in drag with decreasing mass flow from the maximum value of 0.956 down to about 0.850 where the normal shock emerges from the inlet entrance. For further decreases in mass-flow ratio where the spillage through the perforations remains essentially constant, the drag increase is less severe. The region of rapid

drag increase with upstream movement of the normal shock in the perforated region is probably a result of an increase in the force along the limiting streamline $\,S_0\,$ in addition to changes in the cowl pressure drag.

The characteristics of the boundary-layer flow over the external surface of the model were investigated at station 51. With the assumptions that the static pressure measured on the model surface ahead of the rake was constant through the boundary layer and that the total temperature was constant, the rake data were reduced to obtain Mach number profiles, examples of which are shown in figure 8(a). When the analysis in reference 7, (which indicates that the outer limit of the boundary layer is defined by a rapid change in the slope of the Mach number profile) is used, the boundary-layer thickness is less than the rake height for only the maximum mass-flow ratio where the shock is downstream of the perforations. Figure 8(b) shows that by using the point δ of figure 8(a), the data for the highest mass-flow ratio, when converted to dimensionless ratios, are in approximate agreement with the 1/7 power variation associated with turbulent boundarylayer flow.

The boundary-layer thickness determined at a mass-flow ratio of 0.956 by rake measurements at station 51 was approximately 1.03 inches, which is considerably greater than the average value of about 0.60 inch observed on the nonperforated models at the same station. In an attempt to correlate the increased thickness with the mass flow spilled through the perforations, the thickness of the boundary layer at the rake station resulting from mass-flow spillage and friction along the external surface was calculated by the method given in the appendix. The calculated boundary-layer thickness of 1.02 inches is in good agreement with the experimental value. The difference in momentum between stations 3.3 and 51 is approximately equal to the friction force along the surface since the static pressure over this region is relatively constant. The friction-drag coefficient of 0.038 (method given in appendix), based on the maximum frontal area. was slightly smaller than the average value of about 0.045 determined from the nonperforated inlet tests. This result might be expected when the increased boundary-layer thickness is considered along with the decrease in wetted area that results from the omission of the area ahead of station 3.3.

The force on the limiting streamline of the spilled mass flow and on the inside of the cowl to the downstream end of the NACA RM E51B05

perforations was approximated by using assumption (1) in the appendix. This force corresponds to the momentum decrement given by the change of the spilled mass from free-stream velocity to zero axial velocity and in the present case results in a drag coefficient of 0.042 based on the maximum frontal area.

The model external pressure drag was not obtained experimentally because of the lack of pressure instrumentation on the perforated cowl. However, a part of the external pressure distribution was obtained and is shown in figure 9 for a mass-flow ratio of 0.956. Also included in figure 9 is the theoretical pressure distribution for an identical model without perforations and without mass-flow spillage. The theoretical pressure-drag coefficient corresponding to this distribution is 0.036 based on the maximum frontal area. Good agreement of the experimental pressure with theory exists over the rear of the model, but the foremost data points indicate a deviation that is probably associated with the perforation spillage. It appears that any large differences in pressure distribution are confined to the region close to the perforations but since the perforated surface has the greatest slope, any change in pressure distribution over this area results in a relatively large change in pressure drag.

It is possible, on the basis of the values obtained in the appendix, to determine the approximate magnitude of the sum of the pressure and friction forces acting on the external surface from the cowl lip to the downstream end of the perforations. The result obtained is shown graphically in figure 10 where the difference between the total minimum-drag coefficient and the sum of the previously discussed components corresponds to a drag coefficient of approximately 0.040. Because of the relatively small wetted area for this part of the model and consequently a small friction force, it is probable that the greatest part the drag unaccounted for is associated with the change in pressure distribution due to flow spillage over the forward part of the cowl.

This hypothesis suggests that an improvement in the external drag characteristics would be obtained if the spilled mass flow was exhausted through ducts to the external flow over an area parallel to the engine axis where any modifications to the pressure distribution would not cause a pressure drag increase. Another method of reducing the perforation spillage drag is suggested in reference 8 where it is shown that the hole shape may be designed so that, with the shock downstream, no mass passes through the hole to the external flow over the cowl.

NACA RM E51B05

Internal flow characteristics. - The variation of over-all total-pressure recovery, combustion-chamber Mach number, and inlet and subsonic diffuser total-pressure recoveries with mass-flow ratio is presented in figure 11. All total pressures and Mach numbers were computed as discussed in reference 4.

Although the trend of the over-all total-pressure recovery with mass-flow ratio is similar to that of references 4 to 6, the curve differs from those of the nonperforated inlets in that the over-all total-pressure recovery continues to increase after the normal shock passes downstream of the cowl lip until the maximum (critical) mass flow is reached and the shock enters the subsonic diffuser. The mass-flow spillage through the perforations with the shock completely swallowed amounts to about 4.5 percent. The trends of the curves of combustion-chamber Mach number and the inlet and subsonic diffuser total-pressure recoveries as functions of mass-flow ratio are also similar to those of references 4 to 6. It should be noted, however, that the data points at mass-flow ratios of 0.425 and 0.463 for the inlet and subsonic diffuser curves are in the range of shock oscillation and are unreliable. The dashed portions of these curves have been faired to indicate the probable variation that would exist in the total-pressure recoveries without shock oscillation.

The variation of the internal pressure coefficient along the lower surface of the spike and island of the model (θ , 0°) for three mass-flow ratios is presented in figure 12. A general trend of decreasing static pressures with increasing mass-flow ratio can be noted. At m_3/m_0 of 0.956, considerable disturbances exist within the inlet indicating probable shock reflections in the perforated region after the establishment of supersonic flow in the inlet.

Typical Mach number profiles at the entrance to the combustion chember for three mass-flow ratios are presented in figure 13. The largest variations in Mach number across the annular passage occurred at maximum mass flow. In general, the profiles indicate higher velocities close to the shell surface than are obtained close to the spike surface. This phenomenon is probably due to the existence of a thinner boundary layer along the outer shell because of a certain amount of boundary-layer bleed through the perforations. As mentioned in reference 4, the variations in the profiles measured by the various rakes are attributed to the wake effects produced by the support struts.

Effects of Changes in Angle of Attack and Mach Number

External flow characteristics. - The variation of total-drag coefficient with mass-flow ratio for several angles of attack at three Mach numbers is shown in figure 14. The data at a Mach number of 1.99 are presented for only a small range of mass-flow ratios. particularly at angle of attack, because of shock oscillation. For a given angle of attack, the minimum-drag coefficient decreased with increasing Mach number. This variation is primarily associated with a corresponding change in external pressure drag. The value obtained at a Mach number of 1.59 is higher than the other values because the shock did not swallow and therefore includes a component of additive drag associated with flow spillage ahead of the cowl. The drag coefficients are, in general, greater than were obtained for similar test conditions with other models in the investigation. These increases are attributed to the previously discussed adverse effect of spillage through the cowl perforations on the pressure-drag coefficient.

The variations of lift and pitching-moment coefficients with mass-flow ratio for various angles of attack and Mach numbers are presented in figures 15 and 16, respectively. In view of the method of defining the external forces, the lift and pitching moment include the force acting on the limiting streamline of the mass flow passing through the unit in addition to the forces on the internal surface of the cowl in the perforated region. Only small changes in the coefficients with changes in mass-flow ratio are indicated in figures 15 and 16. The experimental center-of-pressure location as affected by changes in mass-flow ratio (fig. 17) is within the range of approximately four to six engine diameters ahead of the base for all angles of attack and Mach numbers investigated.

The variations with angle of attack of the drag, the increment of drag due to angle of attack, the lift, and the pitching-moment coefficients at critical mass-flow ratios for three Mach numbers are shown in figure 18. Also shown are theoretical curves determined by applying the method of reference 9, modified to apply to an open-nose body and neglecting end effects. Comparison of the experimental and theoretical curves shows that the increment of drag and lift coefficient, with the exception of 10° angle of attack at a Mach number of 1.59, are underestimated by the theory whereas the pitching moment is well predicted up to 6° but somewhat overestimated at 10°. The effect of mass-flow spillage through the perforations was not taken into account in the evaluation of

the theoretical curves from the method of reference 9 and therefore close agreement between experiment and theory cannot be expected.

Internal flow characteristics. - The variation of totalpressure recovery and combustion-chamber Mach number with mass-flow
ratio for three free-stream Mach numbers and various angles of
attack is shown in figure 19. It can be noted that the decrease in
pressure recovery with angle of attack is more pronounced on the
perforated inlet than for the inlets reported in references 4 to 6.

Critical mass-flow ratios decrease very slightly with angle of attack up to 6°. The greater decrease in mass-flow ratio at 10° angle of attack for the two higher free-stream Mach numbers is probably due to the normal shock not swallowing completely over the top half of the inlet, which results in greater flow spillage through the perforations or around the outside of the cowl lip. Because the shock does not swallow at all for a free-stream Mach number of 1.59, the decrease in mass flow with increasing angle of attack is very slight. The shock configuration associated with the increased mass-flow spillage due to angle of attack can be observed in the schlieren photographs presented in figure 20.

A plot of the internal pressure coefficient along the lower surface of the spike and island for a constant mass-flow ratio of 0.845 and various angles of attack at a free-stream Mach number of 1.79 is presented in figure 21. In the vicinity of the cowl lip, the pressures indicate a slight downstream movement of the normal shock with increasing angle of attack. Additional internal pressure data are tabulated in table III.

The variation of total-pressure distributions with angle of attack at the entrance to the combustion chamber is shown in figure 22. The trend of the total pressures with angle of attack is not clearly defined, especially at the higher angles of attack. At present, it is unknown whether this condition is the result of asymmetrical flow spillage through the perforations or whether it is associated with shock oscillation.

Performance of Perforations

The average subsonic-flow coefficient of the perforations calculated from the pressure data and continuity relations was approximately 0.53 (M_0 , 1.79; α , 0°). A measured value of throat Mach number was used in the calculations rather than an

assumed value of sonic velocity. This measured value was used because indications of boundary-layer build-up along the spike causing premature choking at the throat were noted while the measured average Mach number at the throat was some subsonic value less than unity. The calculated value of subsonic-flow coefficient is in good agreement with that of reference 2.

SUMMARY OF RESULTS

An investigation of a typical ram-jet configuration utilizing a single-shock spike-type inlet with a perforated cowl was conducted in the Lewis 8- by 6-foot supersonic tunnel at a Reynolds number of approximately 2.4×10⁶ based on the inlet diameter. The investigation was conducted for a range of mass-flow ratios and angles of attack at free-stream Mach numbers of 1.59, 1.79, and 1.99. Force and pressure data were taken and the following results were obtained:

- 1. The use of perforations in the cowl of a spike-type inlet, while giving relatively high pressure recoveries, resulted in rather large drag increases.
- 2. Shock oscillation was encountered at the lower mass-flow ratios for all three free-stream Mach numbers. The range of stable operation decreased with increases in angle of attack and Mach number.
- 3. Decreases in critical mass-flow ratios with increasing angle of attack were more pronounced at the higher free-stream Mach numbers because of associated changes in the inlet shock configuration.
- 4. The average subsonic-flow coefficient of the perforations was approximately 0.53. This value was in good agreement with that obtained in a previous investigation.

Lewis Flight Propulsion Laboratory,
National Advisory Committee for Aeronautics,
Cleveland, Ohio.

APPENDIX

EFFECT OF FLOW SPILLAGE ON BOUNDARY-LAYER CHARACTERISTICS

The analysis of the boundary layer and the spilled mass at the downstream end of the perforations was made by employing the following assumptions:

- (1) The total momentum decrement in the boundary layer at station 3.3 was assumed to be that which corresponds to the product of the spilled mass (assumed to enter the external stream normal to the direction of flow) and the free-stream velocity. The assumption of zero axial velocity of the spilled mass is questionable because the spilled flow does not have to be turned 90° to the stream direction to pass through the perforations. It is therefore implied that the axial momentum of the spilled mass is equal to the defect in momentum due to the boundary-layer flow over the cowl ahead of station 3.3.
- (2) The air passing through the perforations mixed with the free-stream air and the boundary-layer momentum defect at station 3.3 is distributed assuming

$$\frac{\mathbf{u}}{\mathbf{U}} = \left(\frac{\mathbf{y}}{8}\right)^{\frac{1}{7}} \tag{1}$$

that is, the boundary layer at this station is of the same turbulent profile as determined at station 51.

(3) The turbulent boundary-layer thickness increases in accordance with the following relation

$$\delta = \frac{K \left(l_{\Theta} \right)^{\frac{4}{5}}}{\left(\frac{\rho U}{\mu} \right)^{\frac{1}{5}}}$$
 (2)

where K is equal to 0.34, a value that was determined by an analysis of the turbulent boundary-layer growth characteristics obtained from measurements of nonperforated inlets having approximately the same external proportions.

With these three assumptions, the momentum thickness of the boundary layer at station 3.3 was computed and this value was used

to obtain the boundary-layer thickness δ . The effective length of run $l_{\rm e}$, necessary to obtain this value of δ , was determined from equation (2). The length obtained in this manner was added to the distance between stations 3.3 and 51 to obtain the effective value of $l_{\rm e}$ at the rake station. Then using equation (2), the thickness δ the rake station was calculated.

REFERENCES

- 1. Evvard, John C., and Blakey, John W.: The Use of Perforated Inlets for Efficient Supersonic Diffusion. NACA RM E51BlO, 1951 (Revised Version).
- 2. Hunczak, Henry R., and Kremzier, Emil J.: Characteristics of Perforated Diffusers at Free-Stream Mach Number 1.90. NACA RM E50B02, 1950.
- 3. Moeckel, W. E., and Connors, J. F.: Investigation of Shock Diffusers at Mach Number 1.85. III Multiple-Shock and Curved-Contour Projecting Cones. NACA RM E7F13, 1947.
- 4. Esenwein, Fred T., and Valerino, Alfred S.: Force and Pressure Characteristics for a Series of Nose Inlets at Mach Numbers from 1.59 to 1.99. I Conical-Spike All-External Compression Inlet with a Subsonic Cowl Lip. NACA RM E50J26, 1951.
- 5. Obery, L. J., and Englert, G. W.: Force and Pressure Characteristics for a Series of Nose Inlets at Mach Numbers from 1.59 to 1.99. II Isentropic-Spike All-External Compression Inlet. NACA RM E50J26a, 1951.
- 6. Weinstein, Maynard I., and Davids, Joseph: Force and Pressure Characteristics for a Series of Nose Inlets at Mach Numbers from 1.59 to 1.99. III Conical-Spike All-External Compression Compression Inlet with a Supersonic Cowl Lip. NACA RM E50J30, 1951.
- 7. Luidens, Roger W., and Madden, Robert T.: Interpretation of Boundary-Layer Pressure-Rake Data in Flow with a Detached Shock. NACA RM E50I29a, 1950.
- 8. McLafferty, George: Tests of Perforated Convergent-Divergent Diffusers for Multi-Unit Ramjet Application.

 Rep. No. R-53133-19, Res. Dept., United Aircraft Corp.,
 June 1950. (Bur. Aero. Contract NOa(s)-9661, Lot II.)

NACA RM E51B05

2107

9. Allen, H. Julian.: Estimation of the Forces and Moments Acting on Inclined Bodies of Revolution of High Fineness Ratio.
NACA RM A9I26, 1949.

TABLE I - COORDINATES FOR 8-INCH RAM-JET CONFIGURATION

(a) Center-Body Coordinates

Station (in. downstream of cowl lip)	Diameter (in.)
0.5 1.0 1.5 2.0 2.5 3.0 3.5 4.0 5.0 6.0 7.0 7.875 10.0 12.0 14.0 16.0 18.0 20.0 22.0 24.0 26.0 30.031	2.657 3.020 3.383 3.734 4.027 4.265 4.365 4.365 4.525 4.575 4.600 4.585 4.545 4.486 4.415 4.327 4.220 4.084 3.922 3.715 3.343

(b) Outer-Shell Coordinates

Station (in. downstream	Diameter (in.)				
of cowl lip)	External	Internal			
0.5 1.0 2.0 3.0 4.0 4.5 5.0 8.875 9.875 22.0 30.0 32.0	5.855 6.045 6.330 6.538 6.670 6.714 6.750 6.947 6,998 7.616 8.024 8.125	5.712 5.850 6.100 6.302 6.430 6.470 6.500 6.697 6.748 7.366 7.774 7.875			
	. •	NACA			

TABLE II - LOCATION OF STATIC-PRESSURE
ORIFICES ON PRESSURE MODEL

Station (in. downstream of cowl lip; negative values indicate in. upstream of cowl lip)							
External shell orifices	, -	rnal					
(a)	Spike	Island					
11.0 12.0 14.0 16.0 18.0 21.0 24.0 27.0 31.0 35.0 40.0	-1.5 -1.0 -0.5 0.0 0.5 1.0 1.5 2.0 2.5 3.0 4.0 5.0 6.0	8.0 9.0 10.0 11.0 12.0 14.0 16.0 18.0 21.0 24.0 27.0 31.0 37.0					

^aTwo rows of orifices at $\theta = 180^{\circ}$ and $\theta = 270^{\circ}$.

 $b\theta = 00$.

TABLE III - EXTERNAL AND INTERNAL PRESSURE DISTRIBUTIONS OF NACA 8-INCH RAM JET CONFIGURATION FOR FOUR ANGLES OF ATTACK AT FREE-STREAM MACH NUMBER OF 1.79

(a) Angle of attack, 0°.

Sta- tion	r	$m_3/m_0 = 0.956$ $m_3/m_0 = 0.847$									$m_3/m_0 = 0.682$				
	Longitudinal distribution of Cp														
	Outer shell, external			enter body	Outer shell, external		,	Center body	Outer shell, external			Center			
⊖ →	180°	270	0	00	180°	270	0	00	1800	270	,0	00			
-1.5 -1.0 -0.5 0 0.5 1.0 1.5 2.0 2.5 3.0 4.0 5.0 6.0 7.0 8.0 9.0 10.0 11.0 12.0 14.0 12.0 12.0 24.0 27.0 31.0 24.0 27.0 31.0 27.0 24.0 27.0 27.0 27.0 27.0 27.0 27.0 27.0 27	-0.006 004 002 001 .004 .006 .010 .004 017 010		009	0.328 .302 .351 .345 .363 .600 .471 .958 .633 .631 .561 .725 .940 .933 .993 1.081 1.217 1.314 1.388 1.483 1.563 1.651 1.651	-0.016014012001004001 .004019010		019 013 007 009 004 004 002	0.328 .303 .355 .429 1.112 1.238 1.190 1.172 1.122 1.294 1.304 1.335 1.330 1.355 1.330 1.359 1.461 1.511 1.513 1.661 1.665 1.717	-0.024 022 019 016 002 002 001 022		027 022 015 017 010 009	0.328 .364 .594 1.021 1.305 1.344 1.348 1.511 1.524 1.532 1.540 1.540 1.532 1.556 1.594 1.628 1.701 1.772 1.783			
Sta- tion	Outer shell, external			T	r shell		on of (P	r shell	, exte	rnal				
⊖ →	1980	2160	2340	2520	1980	2160	2340	2520	1980	2160	2340	2520			
14.0	-0.002 012	-0.004 012	-0.007 012	-0.002	-0.012 012	-0.016 012	-0.017 013		-0.019 014	-0.022 014	-0.023				

NACA

3

TABLE III - EXTERNAL AND INTERNAL PRESSURE DISTRIBUTIONS OF NACA 8-INCH RAM-JET CONFIGURATION FOR FOUR ANGLES OF ATTACK AT FREE-STREAM MACH NUMBER OF 1.79 - Continued

Sta- tion		$m_3/m_0 = 0.946$					$m_3/m_0 = 0.888$				$m_3/m_0 = 0.836$			
				Long	itudina	l dist	ributio	on of Cp						
		Outer shell, external			Outer shell, external		ell,	Center body	Outer shell, external			Cente		
9 -	180	0 2	2700	00	180	0	270°	00	180	0. 2	2700	00		
-1.5 -1.0 -0.5 0 0.5 1.0 1.5 2.5 2.5 2.5 4.0 9.0 10.0 11.0 11.0 11.0 11.0 11.0 11.	-0.02 03 03 06 06 06 02 03	23 - 20 - 10 - 20 - 20 - 20 - 20 - 20 - 20	.018 .016 .012 .008 .008 .007 .008 .003 .002	0.395 .367 .421 .418 .433 .505 .115 .579 .581 .669 .678 .655 .554 .460 .894 .904 .904 .904 .1.290 .1.364 .1.461 .1.541 .1.595 .1.632	-0.00 00 00 00 00 00 00 0	30 27 17 13 06 01 02 04 01 22	0.023 022 018 014 012 012 006 004	0.392 .365 .418 .414 .428 .432 .504 1.007 1.095 1.216 1.234 1.265 1.269 1.310 1.308 1.328 1.364 1.438 1.438 1.499 1.546 1.671 1.704 1.732	-0.03 03 03 00 00 00 00 01 01	35	.028 .027 .022 .017 .017 .012 .007 .004	0.39 .36 .41 .41 .93 .1.18 1.20 1.17 1.10 1.28 1.29 1.30 1.31 1.30 1.33 1.37 1.44 1.50 1.54 1.66 1.70 1.72		
1.			- 11					ion of	1		2.2			
Sta- tion	Ot	iter sh	e11, e	xternal	Ot	iter s	nell, e	external	01	ter sh	ell, e	xterna		
→	198°	216°	234°	252°	198°	216°	2340	2520	198°	216°	2340	252		
14.0	-0.015 013	-0.018 013	-0.02		-0.021 015	-0.02		-0.013	-0.025 017					

NACA

TABLE III - EXTERNAL AND INTERNAL PRESSURE DISTRIBUTIONS OF NACA 8-INCH RAM-JET CONFIGURATION FOR FOUR ANGLES OF ATTACK AT FREE-STREAM MACH NUMBER OF 1.79 - Continued

(c) Angle of attack, 6°.

Sta- tion	1	$m_3/m_0 = 0.937$ $m_3/m_0 = 0.914$									$m_3/m_0 = 0.830$			
01011				Longit	udinal	distrib	ution	of C_p						
	Outer shell, external			enter body	Outer shell, external			Center body	Outer shell, external			enter oody		
θ →	1800	27	00	0°	180°	270	0	00	180°	270	00	00		
-1.5 -1.0 -0.5 0 0.5 1.0 2.5 3.0 2.5 3.0 6.0 7.0 8.0 9.0 10.0 11.0 12.0 12.0 12.0 21.0 21.0 21	-0.03 02 01 00 00 00 00	55	.035 .038 .038 .038 .038 .038 .038 .034	0.463 .437 .495 .504 .507 .507 .624 .545 .495 .630 .619 .598 .517 .892 .969 .985 1.027 1.091 1.199 1.279 1.345 1.433 1.565 1.606	-0.037 029 021 012 002 003 001 022		041 040 040 038 038 038	0.466 .440 .497 .506 .510 .500 .418 .476 .635 .635 .858 1.087 1.117 1.144 1.219 1.254 1.261 1.281 1.317 1.390 1.448 1.496 1.563 1.626 1.665 1.698 1.722	-0.043 035 026 017 010 003 003 003 011 011		043 044 043 040 0339 0339 034	0.464 .438 .495 .504 .511 .930 .897 .970 1.060 1.261 1.268 1.274 1.297 1.297 1.283 1.294 1.342 1.422 1.453 1.609 1.669 1.706 1.750		
				Circumf	erential	distr	butio	on of Cp						
Sta- tion	Outer	Outer shell, external			Outer	Outer shell, external			Outer shell, exter			nal		
θ→	198°	2160	2340	252°	1980	2160	2340	2520	198°	2160	234°	2520		
14.0	-0.025 018	-0.032 022	-0.045 029	-0.039 041	-0.026 018	-0.033	-0.04			-0.035 021	-0.048 028			

TABLE III - EXTERNAL AND INTERNAL PRESSURE DISTRIBUTIONS OF NACA 8-INCH RAM-JET CONFIGURATION FOR FOUR ANGLES OF ATTACK AT FREE-STREAM MACH NUMBER OF 1.79 - Concluded

(d) Angle of attack, 100,

Sta- tion		m3/m0 =	= 0.89	97	$m_3/m_0 = 0.857$					
01011		Longit	udina	al distri	bution	of Cp				
	Outer shell, Center external body				0	Outer shell, external				
θ→	1800	180° 270° 0°		180	0	270°		00		
-1.5 -1.0 -0.5 0 0.5 1.0 1.5 2.0 2.5 3.0 4.0 5.0 6.0 9.0 10.0 11.0 12.0 14.0 12.0 14.0 24.0 27.0 35.0 35.0 40.0 40.0 40.0 40.0 40.0 40.0 40.0 4	-0.045 036 024 014 008 004 036 036 026	5	.075 .083 .088 .091 .101 .104 .099 .088	0.554 .545 .608 .599 .605 .807 .413 .030 .593 .487 .501 .510 .456 .382 .396 .581 .629 .471 .312 .188 .482 .711 .907 1.045 1.131 1.187	-0.0 0 0 0 0 0 0	48 39 24 14 07 02 01 04 02 28	0.075 082 089 090 101 102 101 096		0.549 .539 .602 .595 .613 .771 .386 .584 .754 1.035 1.080 1.164 1.194 1.234 1.234 1.248 1.348 1.348 1.348 1.492 1.548 1.585 1.612	
	Circumferential distribution of Cp									
Sta- tion	Outer	shell	, exte	ernal	Oute	r shel	l, ext	ern	al	
θ→	1980	2160	234	2520	1980	2160	234	0	2520	
14.0	-0.031 042	-0.049 043	-0.0°	78 -0.1 03					-0.100 060	

NACA

		-
		*
		*
		;
		·
		•

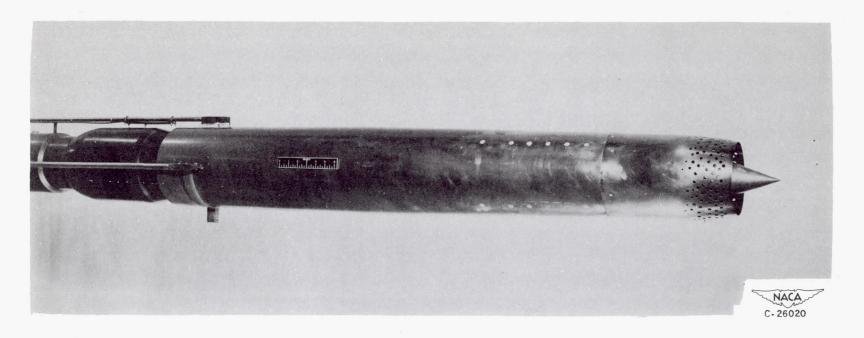
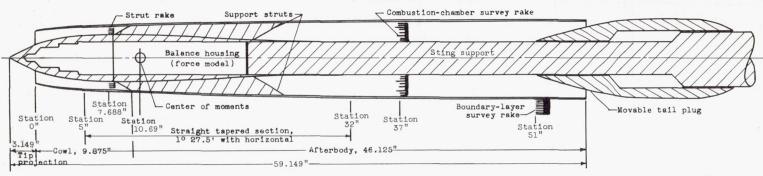


Figure 1. - Pressure model of NACA 8-inch ram-jet configuration with external-internal compression inlet utilizing perforations.



(a) NACA 8-inch ram-jet configuration.

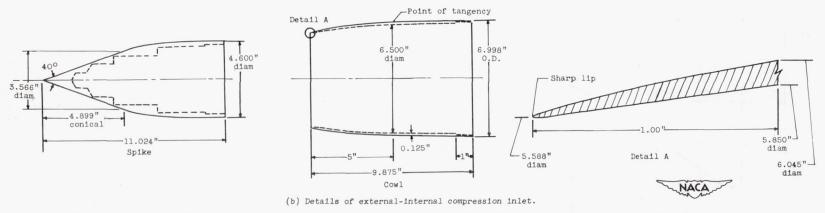


Figure 2. - Schematic diagram of NACA 8-inch ram-jet configuration showing principal dimensions of model and details of inlet.

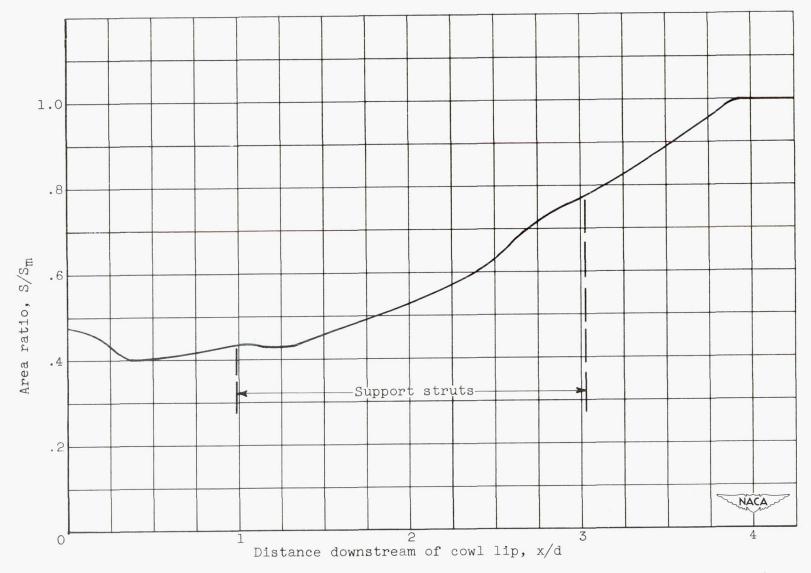


Figure 3. - Longitudinal variation of mean geometric area.

SIOT

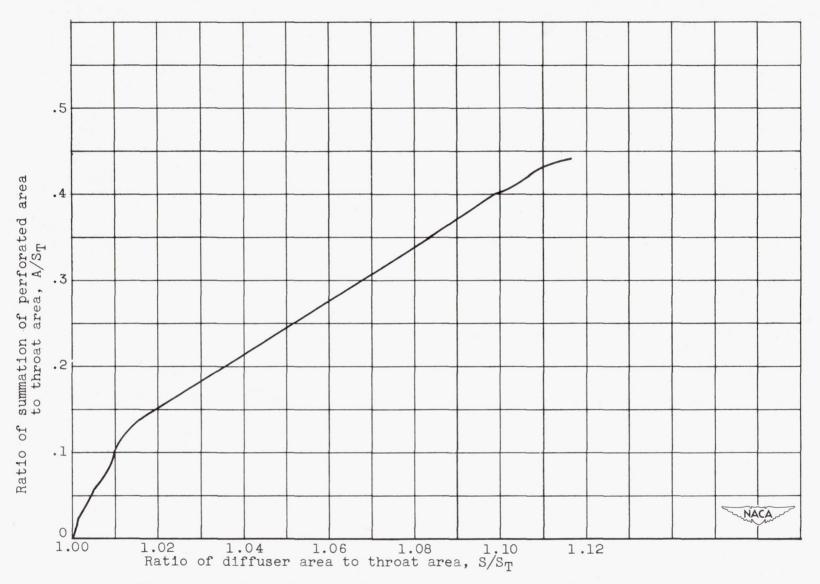


Figure 4. - Distribution of perforations along diffuser inlet.

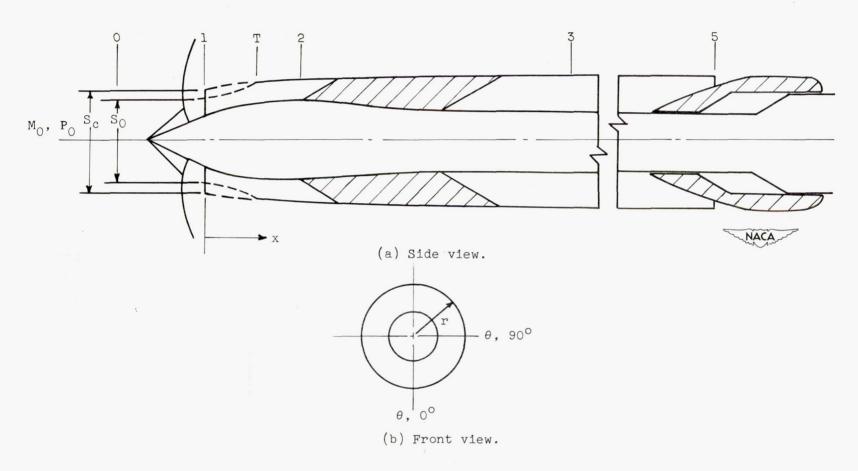
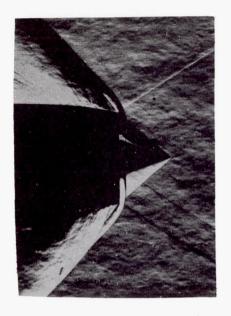
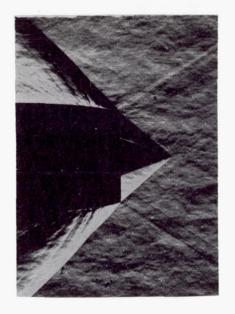
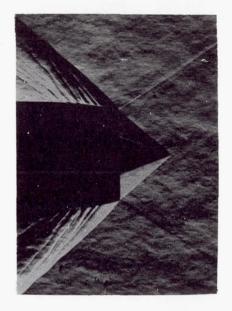


Figure 5. - Notation for 8-inch ram-jet configuration.







- (a) Mass-flow ratio, 0.683.
- (b) Mass-flow ratio, 0.871.

(c) Mass-flow ratio, 0.956.

Figure 6. - Typical schlieren photographs at zero angle of attack and free-stream Mach number of 1.79.

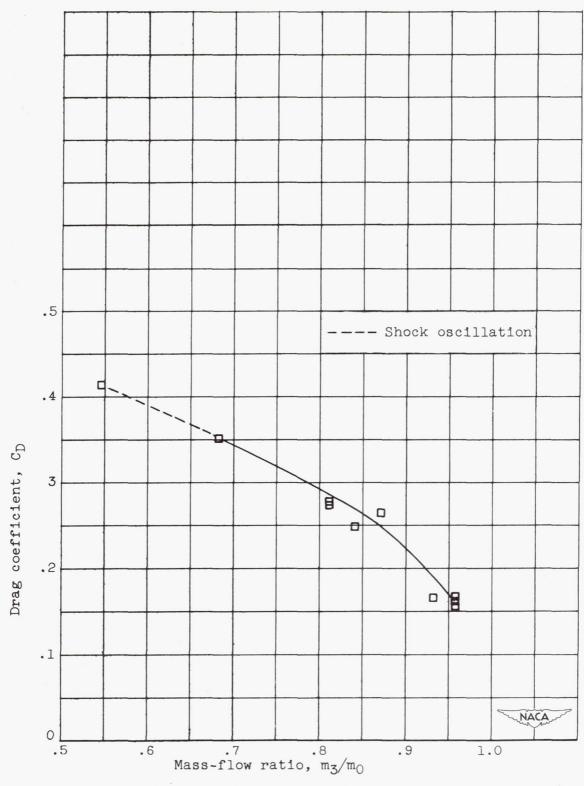
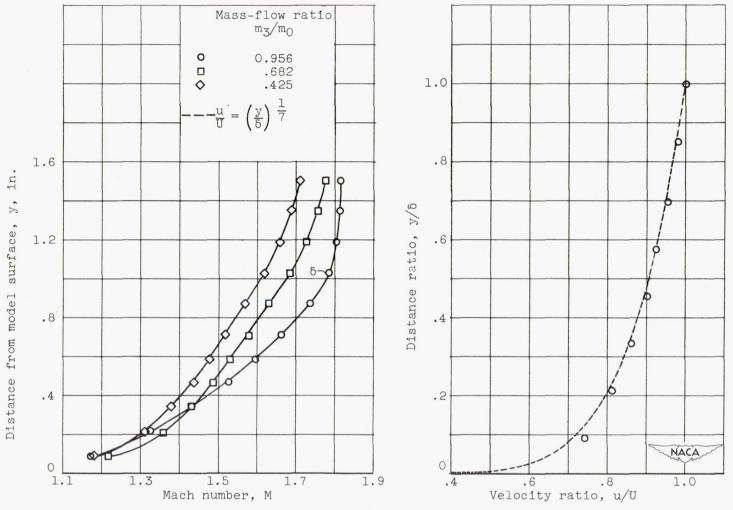


Figure 7. - Variation of total-drag coefficient with mass-flow ratio. Angle of attack, 0° ; free-stream Mach number, 1.79.



(a) Variation of Mach number distribution with (b) Comparison of experimental and theoretmass-flow ratio. (cal boundary-layer profile.

Figure 8. - Typical external boundary-layer profiles at station 51 for free-stream Mach number of 1.79 and angle of attack of 0° .

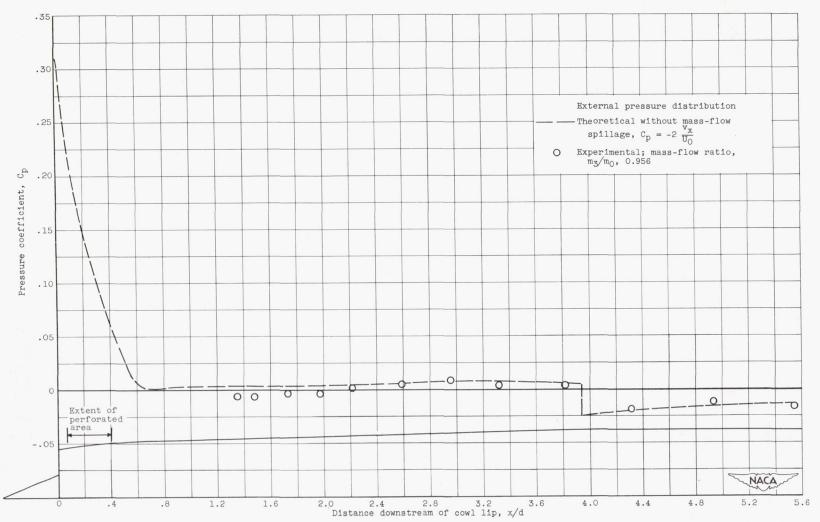


Figure 9. - Longitudinal variation of external pressure coefficient at free-stream Mach number of 1.79 and angle of attack of 0° .

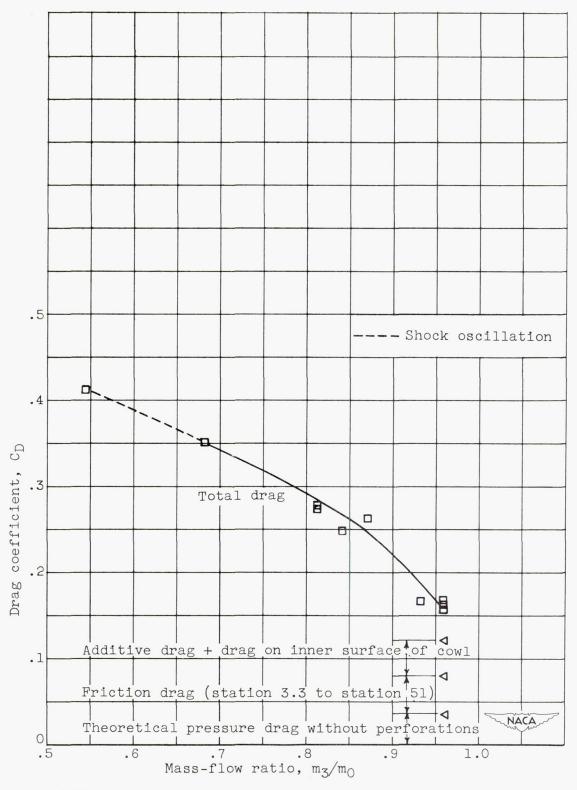


Figure 10. - Drag characteristics at free-stream Mach number of 1.79 and angle of attack of 0° .

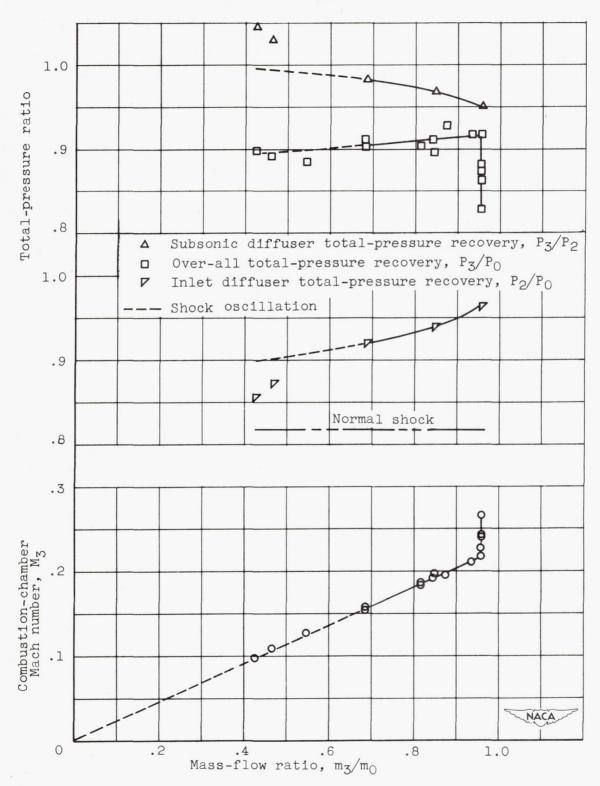


Figure 11. - Variation of total-pressure recovery and combustion-chamber Mach number with mass-flow ratio at free-stream Mach number of 1.79 and angle of attack of 0°.

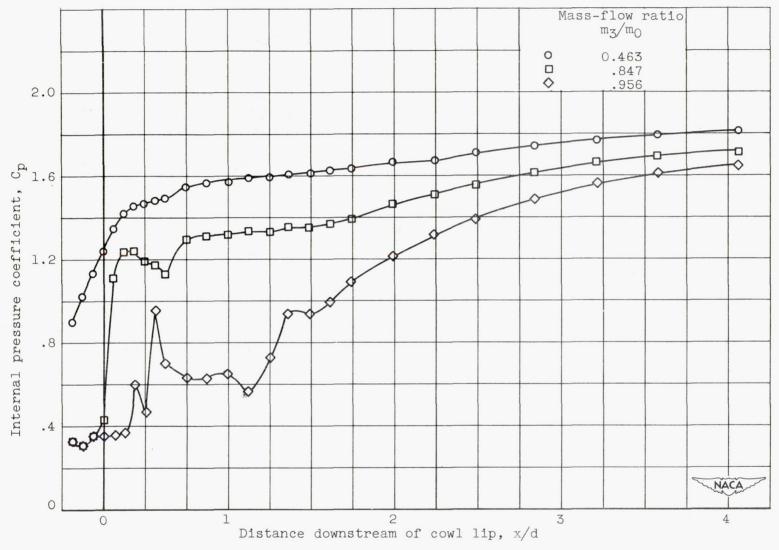


Figure 12. - Longitudinal variation of internal pressure coefficients along lower surface of model spike and island at free-stream Mach number of 1.79 and angle of attack of 0° .

NACA RM E51B05

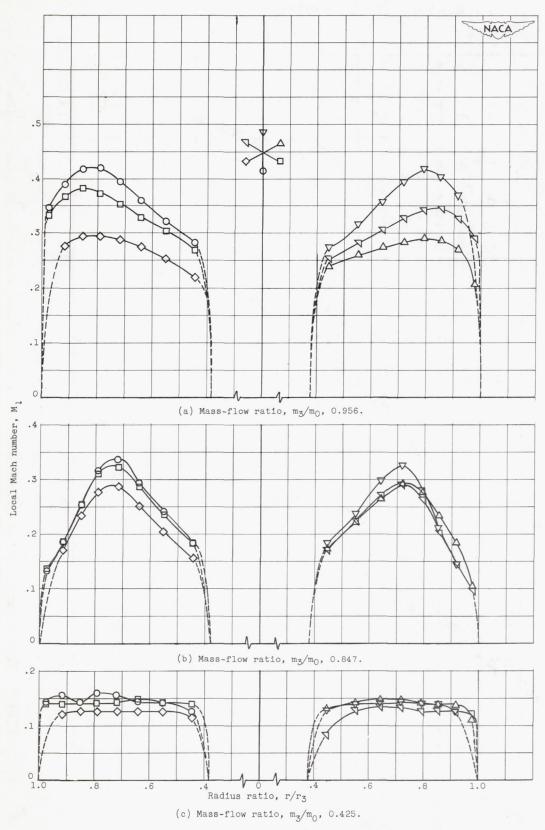


Figure 13. - Variation of Mach number distribution at entrance to combustion chamber for three mass-flow ratios at free-stream Mach number of 1.79 and angle of attack of 0°.

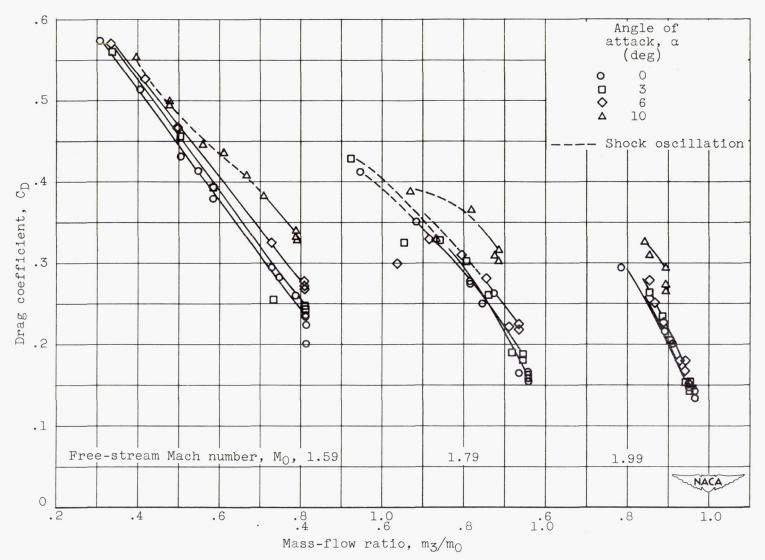


Figure 14. - Variation of total-drag coefficient with mass-flow ratio at four angles of attack for three free-stream Mach numbers.

•

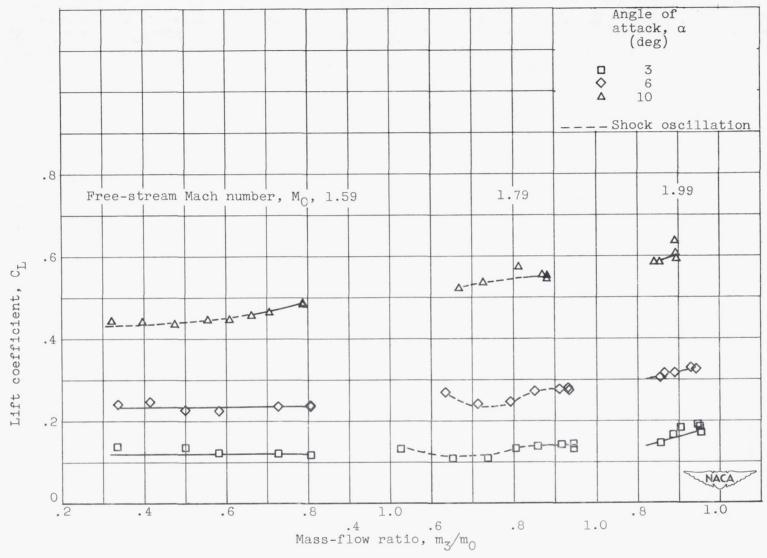


Figure 15. - Variation of external lift coefficients with mass-flow ratio at three angles of attack for three free-stream Mach numbers.

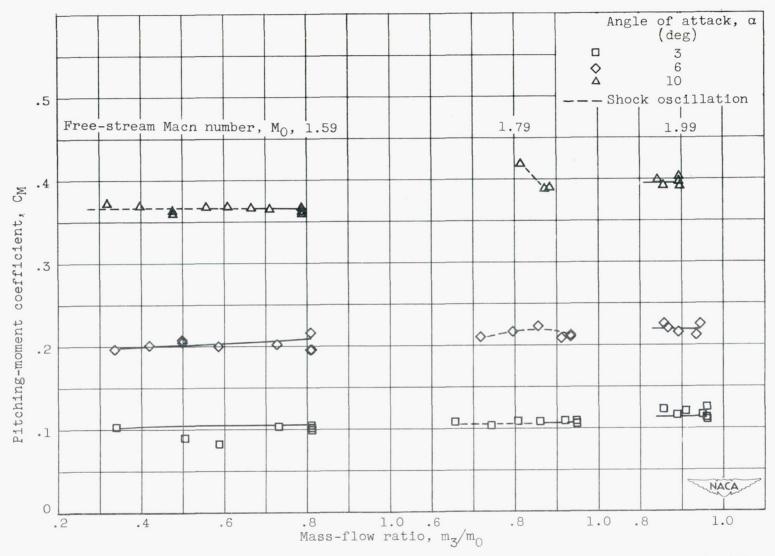


Figure 16. - Variation of external pitching-moment coefficients about base of model with mass-flow ratio at three angles of attack for three free-stream Mach numbers.

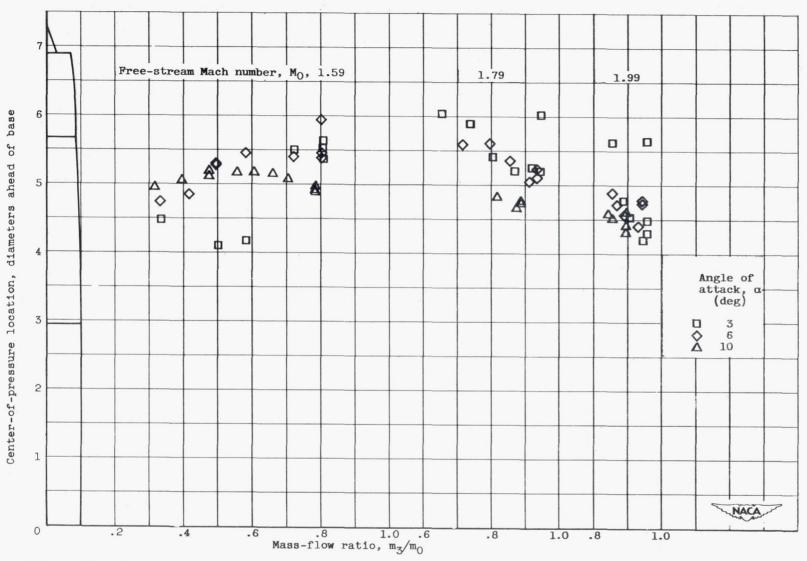


Figure 17. - Variation of center-of-pressure location with mass-flow ratio at three angles of attack for three free-stream Mach numbers.

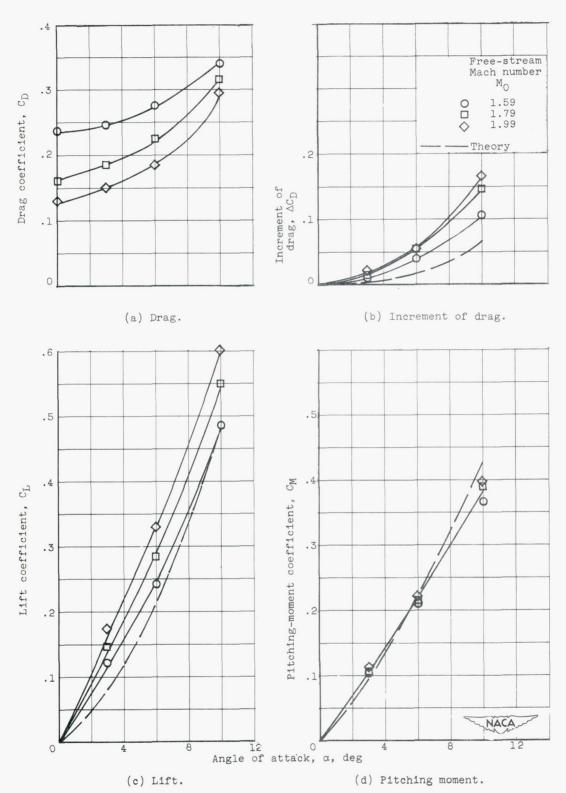


Figure 18. - Variation of drag, increment of drag, lift, and pitching-moment coefficients with angle of attack at critical mass-flow ratios for three free-stream Mach numbers.

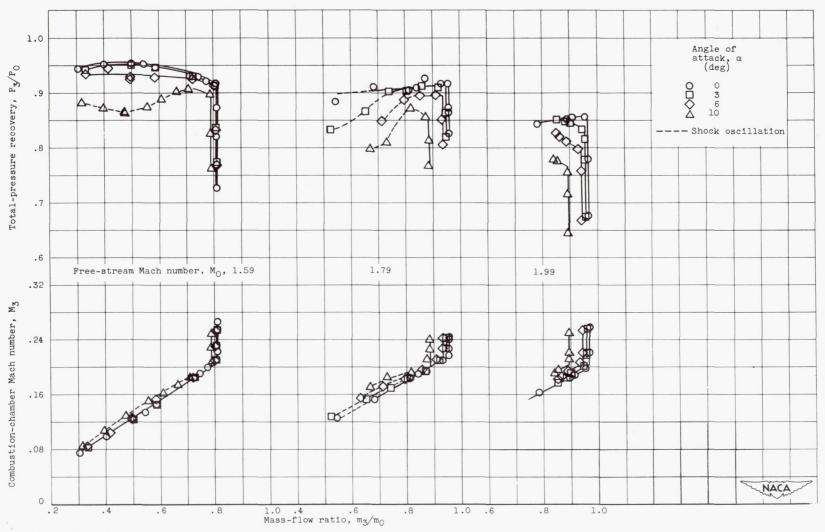
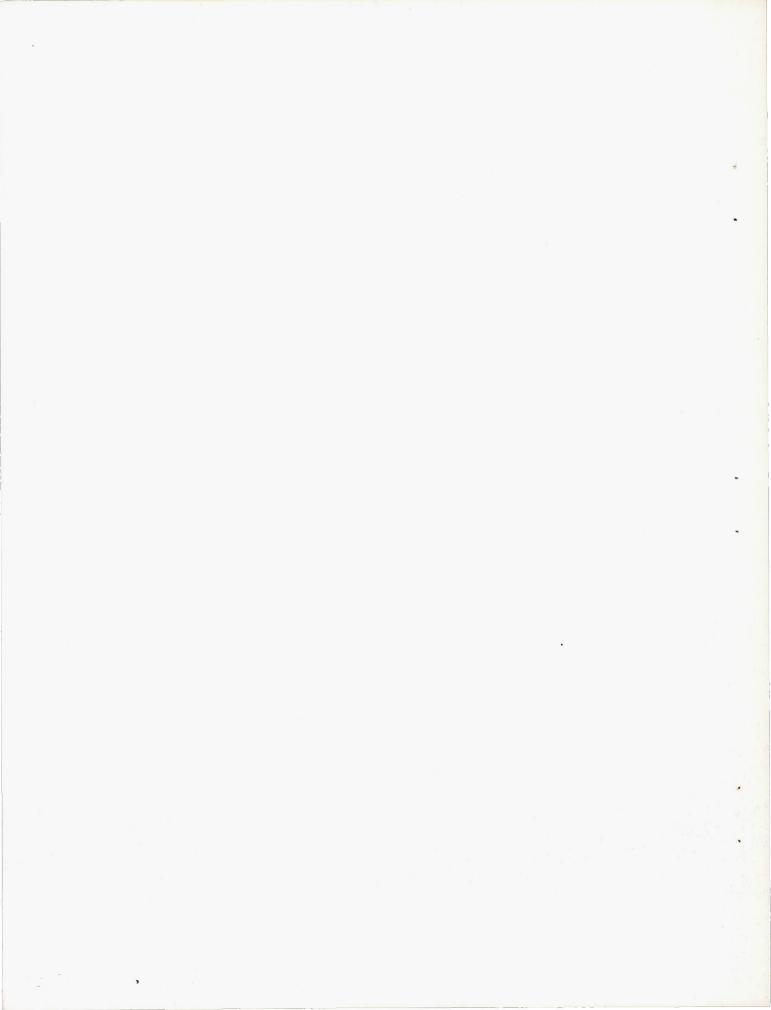
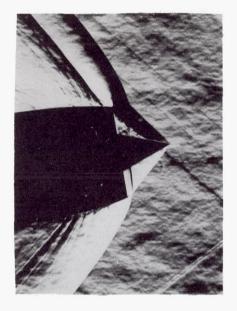
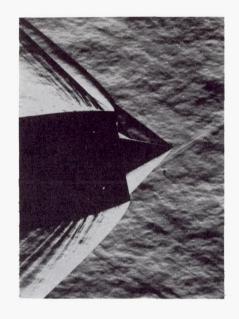
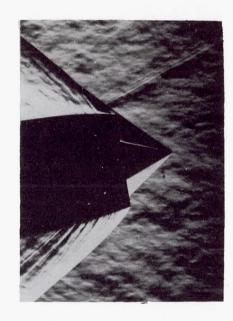


Figure 19. - Variation of total-pressure recovery and combustion-chamber Mach number with mass-flow ratio for various angles of attack and three free-stream Mach numbers.





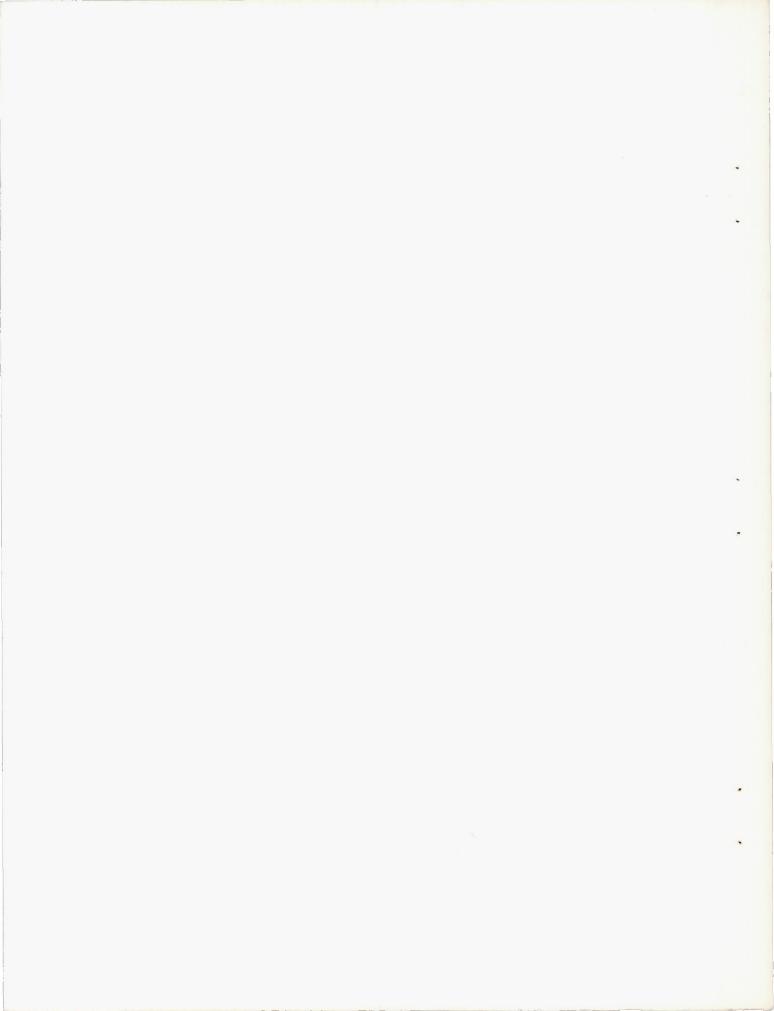




C- 27098

- (a) Mass-flow ratio, 0.708; freestream Mach number, 1.59
- (b) Mass-flow ratio, 0.883; freestream Mach number, 1.79.
- (c) Mass-flow ratio, 0.893; freestream Mach number, 1.99.

Figure 20. - Typical schlieren photographs at angle of attack of 10°.



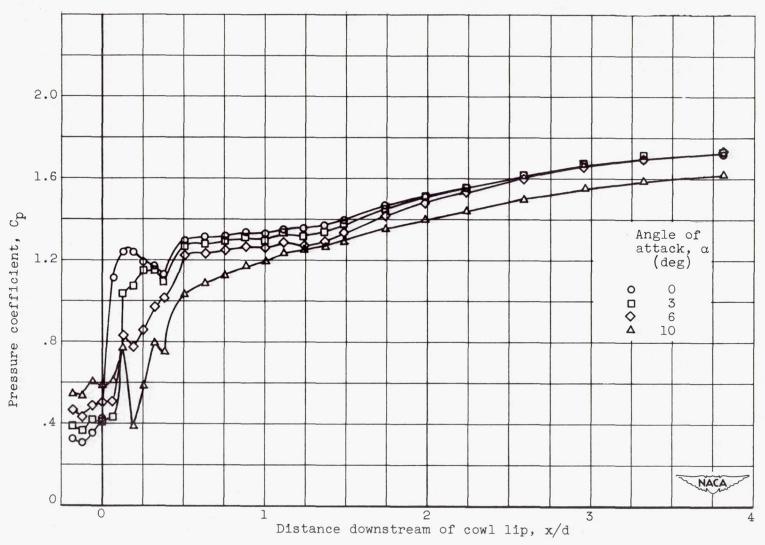


Figure 21. - Longitudinal variation of internal pressure coefficients along lower surface of model spike and island for constant mass-flow ratio of 0.845 at free-stream Mach number of 1.79 for four angles of attack.

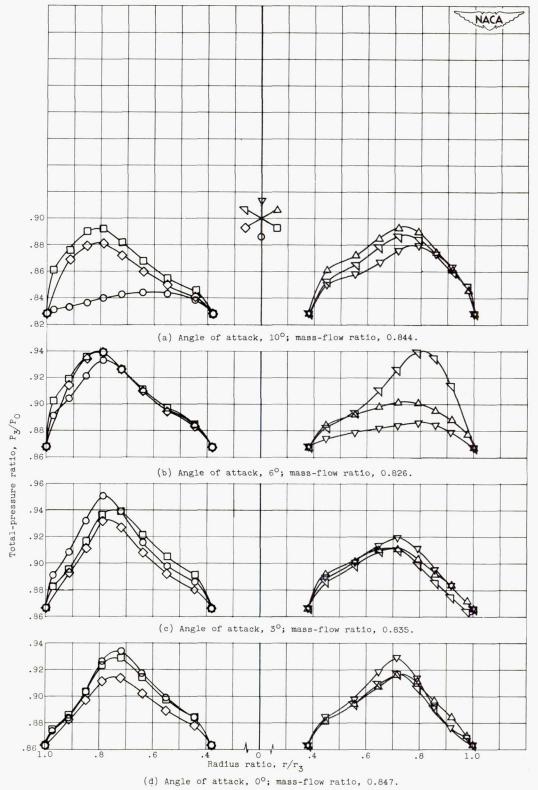


Figure 22. - Variation of total-pressure distribution at entrance to combustion chamber for approximately constant mass-flow ratio at free-stream Mach number of 1.79 and for four angles of attack.